

AD-A082 204

DAVID W TAYLOR NAVAL SHIP RESEARCH AND DEVELOPMENT CE--ETC F/6 11/8
FRICTION CHARACTERISTICS OF WATER-LUBRICATED STAVE BEARINGS. (U)

FEB 80 T L DAUGHERTY, N T SIDES

DTNSROC-80/023

UNCLASSIFIED

NL

1 OF 1
AD-A082 204



END

DATE

FILED

4-80

DTIC

ADA082204

UNCLASSIFIED

SECURITY CLASSIFICATION OF THIS PAGE (When Data Entered)

REPORT DOCUMENTATION PAGE		READ INSTRUCTIONS BEFORE COMPLETING FORM
1. REPORT NUMBER DTNSRDC-86/023	2. GOVT ACCESSION NO.	3. RECIPIENT'S CATALOG NUMBER
4. TITLE (and Subtitle) 6 FRICTION CHARACTERISTICS OF WATER-LUBRICATED STAVE BEARINGS	5. TYPE OF REPORT & PERIOD COVERED 9 Research and Development <i>rept.</i>	
7. AUTHOR(s) 10 Thomas L. Daugherty Nathan T. Sides	6. PERFORMING ORG. REPORT NUMBER	
9. PERFORMING ORGANIZATION NAME AND ADDRESS David W. Taylor Naval Ship R&D Center Bethesda, MD 20084	8. CONTRACT OR GRANT NUMBER(s)	
11. CONTROLLING OFFICE NAME AND ADDRESS David W. Taylor Naval Ship R&D Center Annapolis, MD 21402	10. PROGRAM ELEMENT, PROJECT, TASK AREA & WORK UNIT NUMBERS 17 Program Element 62766N Task Area ZF 61512001 Work Unit 2052-122	
14. MONITORING AGENCY NAME & ADDRESS (if different from Controlling Office) 16 F61512	12. REPORT DATE 11 Feb 1986	
16. DISTRIBUTION STATEMENT (of this Report) APPROVED FOR PUBLIC RELEASE; DISTRIBUTION UNLIMITED.	13. NUMBER OF PAGES 33	
17. DISTRIBUTION STATEMENT (of the abstract entered in Block 20, if different from Report)	15. SECURITY CLASS. (of this report) UNCLASSIFIED	
18. SUPPLEMENTARY NOTES	15a. DECLASSIFICATION/DOWNGRADING SCHEDULE	
19. KEY WORDS (Continue on reverse side if necessary and identify by block number) Friction Rubber Bearings Bearings Inverse Hydrodynamic Lubrication Stave Bearings Water Lubrication		
20. ABSTRACT (Continue on reverse side if necessary and identify by block number) Experimental friction data for full-complement water-lubricated stave bearings are presented and discussed. The bearings used in the study are of similar construction to those used by the U.S. Navy for propulsion shaft support in outboard locations such as sterntube and strut bearings. Break-away friction characteristics are compared for seven stave designs under a (Continued on reverse side)		

DD FORM 1 JAN 73 1473

EDITION OF 1 NOV 65 IS OBSOLETE
S/N 0102-LF-014-6601

UNCLASSIFIED

SECURITY CLASSIFICATION OF THIS PAGE (When Data Entered)

387682

Lur

UNCLASSIFIED

SECURITY CLASSIFICATION OF THIS PAGE (When Data Entered)

(Block 20 continued)

load of 280 kilopascals (40 pounds per square inch). The duration of load was varied from 1 minute to almost 70 hours. Dynamic friction results also are presented for each stave design under loads of 70, 280, and 700 kilopascals (10, 40, and 100 pounds per square inch, respectively) in incremental speeds up to 3.6 meters per second (700 feet per minute). The seven stave designs included two rubber compositions, two rubber hardnesses, two types of backing material, and geometrical variations. Rubber thickness and other geometrical changes had the most significant influence on dynamic friction. No correlation between static and dynamic friction was apparent.

Accession For	
NTIS ORA&I	<input checked="checked" type="checkbox"/>
DDC TAB	<input type="checkbox"/>
Unannounced	<input type="checkbox"/>
Justification	
By	
Distribution	
Availability	
Dist.	Available for special
A	

UNCLASSIFIED

SECURITY CLASSIFICATION OF THIS PAGE (When Data Entered)

TABLE OF CONTENTS

	Page
LIST OF FIGURES.	iii
LIST OF TABLES	iv
NOMENCLATURE	v
LIST OF ABBREVIATIONS.	vii
ABSTRACT	1
ADMINISTRATIVE INFORMATION	1
INTRODUCTION	1
THEORETICAL BACKGROUND	4
BEARING STAVE DESCRIPTION.	7
TEST MACHINE	9
TEST PROCEDURE	12
RESULTS.	13
DISCUSSION AND CONCLUSIONS	18
APPENDIX - CORRECTION TORQUE CALCULATION	23
REFERENCES	27

LIST OF FIGURES

1 - Typical Bearing Construction	3
2 - Typical Dynamic Friction Coefficient for Water-Lubricated Stave Bearing Before and After Break-In.	5
3 - Stave Configuration and Identification	8
4 - Test Machine	10
5 - Top View of Test Bearing	11

	Page
6 - Dynamic Friction Coefficient for Conventional Staves.	14
7 - Breakaway Friction versus Time under 280-kPa (40-psi) Load for Conventional Staves	17
8 - Load Pattern on Set 1 after 50-hr Break-In at 60 rpm under 280-kPa (40-psi) Load.	19
9 - Track Width and Load Distribution for Set 1 after 50-hr Break-In at 60 rpm and 28-kPa (40-psi) Load	20
10 - Support Bearing and Seal Arrangement.	24

LIST OF TABLES

1 - Dynamic Friction Characteristics.	15
2 - Static Coefficient of Friction under 280-kPa (40-psi) Load	16

NOMENCLATURE

a	Half the width of the contact area, cm (in.)
D	Bearing diameter, cm (in.)
$\frac{dp}{dx}$	Rate of pressure change with distance in the x direction, Pa/cm (psi/in.)
f	Coefficient of friction
f_{min}	Minimum coefficient of friction
h	Film thickness, cm (in.)
h^*	Film thickness at point of maximum pressure, cm (in.)
L	Bearing length, cm (in.)
P	Test bearing load, N (lb)
p	Pressure in lubricant film, Pa (psi)
R	Radius of journal, cm (in.)
R_1	Load reaction on 3l4 size support bearing, N (lb)
R_2	Load reaction on 2l4 size support bearing, N (lb)
T	Bearing torque, N-cm (lb-in.)
T_B	Total torque from support and calibration ball bearings, N-cm (lb-in.)
T_{CB}	Torque of calibration bearing, N-cm (lb-in.)
T_L	Ball bearing torque due to load, N-cm (lb-in.)
T_S	Seal torque, N-cm (lb-in.)
T_{SB}	Support bearing torque, N-cm (lb-in.)
T_T	Total measured torque, N-cm (lb-in.)
T_{TARE}	Tare torque of machine support bearings and seal, N-cm (lb-in.)
T_V	Viscous ball bearing torque, N-cm (lb-in.)

- U Velocity of the mating surface past the bearing surface, cm/sec
 (in./sec)
- W Load per unit width, N/cm (lb/in.)
- x Distance in x direction, cm (in.)
- y Distance in y direction, cm (in.)
- μ Viscosity of the lubricant, $\frac{N-s}{m^2}$ (reyn)

LIST OF ABBREVIATIONS

cm	Centimeter
kPa	Kilopascal
m/s	Meter per second
N-m	Newton-meter
O.D.	Outside diameter
psi	Pound per square inch
rpm	Revolution per minute
μin.	Microinch

ABSTRACT

Experimental friction data for full-complement water-lubricated stave bearings are presented and discussed. The bearings used in the study are of similar construction to those used by the U.S. Navy for propulsion shaft support in outboard locations such as sterntube and strut bearings. Breakaway friction characteristics are compared for seven stave designs under a load of 280 kilopascals (40 pounds per square inch). The duration of load was varied from 1 minute to almost 70 hours. Dynamic friction results also are presented for each stave design under loads of 70, 280, and 700 kilopascals (10, 40, and 100 pounds per square inch, respectively) in incremental speeds up to 3.6 meters per second (700 feet per minute). The seven stave designs included two rubber compositions, two rubber hardnesses, two types of backing material, and geometrical variations. Rubber thickness and other geometrical changes had the most significant influence on dynamic friction. No correlation between static and dynamic friction was apparent.

ADMINISTRATIVE INFORMATION

This report covers work conducted under DTNSRDC In-House Independent Exploratory Development, Program Element 62766N, Task Area ZF 61512001, Work Unit 2832-122.

The work covered in this report will be presented at the 1980 Annual Meeting of the American Society of Lubrication Engineers (ASLE) and later will be published in ASLE Transactions.

INTRODUCTION

Inboard and outboard bearings support main propulsion shafting in ships. The outboard bearings are classified as sterntube and strut bearings. Their primary function is to support the propeller and shaft while permitting rotation of the shaft. While sterntube and strut bearings in most commercial ships are oil-lubricated, they are lubricated by seawater in the majority of U.S. Navy ships. Oil-lubricated bearings inherently have more load capacity than those lubricated with seawater because oil viscosity is about 100 times that of water. However, oil-lubricated outboard bearings are prone to seal failure and oil leakage.

The water-lubricated sterntube and strut bearings used by the U.S. Navy generally consist of bronze bearing shells, made in halves and lined with a suitable wearing material. Each bearing half is grooved longitudinally with a series of dovetail slots, in which bearing staves can be inserted (Figure 1). Each stave is made of or faced with an appropriate wearing material such as lignum vitae, laminated phenolic, or rubber. These bearings operate completely submerged in seawater with limited water flow in the grooves between adjacent staves. A corrosion-resistant sleeve made of gunmetal, copper-nickel, or similar material is installed over the shaft at the bearing. The predominant bearing stave used today is flat-surfaced synthetic rubber bonded to a naval brass backing. Both lignum vitae and the laminated phenolics are used less commonly today because of their higher wear rates and undesirable swelling characteristics. Natural rubber staves are no longer used because they tended to fail catastrophically by a mode referred to as "blow outs."^{1*}

The bonded synthetic staves used today must satisfy the requirements of MIL-B-17901.² The hardness of the rubber surface is specified using the Shore A durometer scale as 85 ± 5 (instantaneous). Stave bearings are designed to a maximum unit loading of $280-310 \text{ kPa}^{**}$ (40-45 psi) with an L/D ratio of 3 to 4. Clearances of approximately 0.003 cm/cm (0.003 in./in.) diameter are used for new installations. Allowance must also be made to reduce misalignment effects caused by shaft deflections due to the overhung propeller. The aft sterntube bearing therefore is often mounted in an annular rubber sleeve which provides flexibility, allowing the bearing housing to align itself to the shaft.

Problems which currently exist with water-lubricated rubber-surfaced stave bearings are:

1. inadequate bonding between the surface rubber and the brass backing - resulting in potential loss of wear surface and subsequently bearing failure;

* A complete listing of references is given on page 27.

** Definitions of abbreviations used are given on page vii.

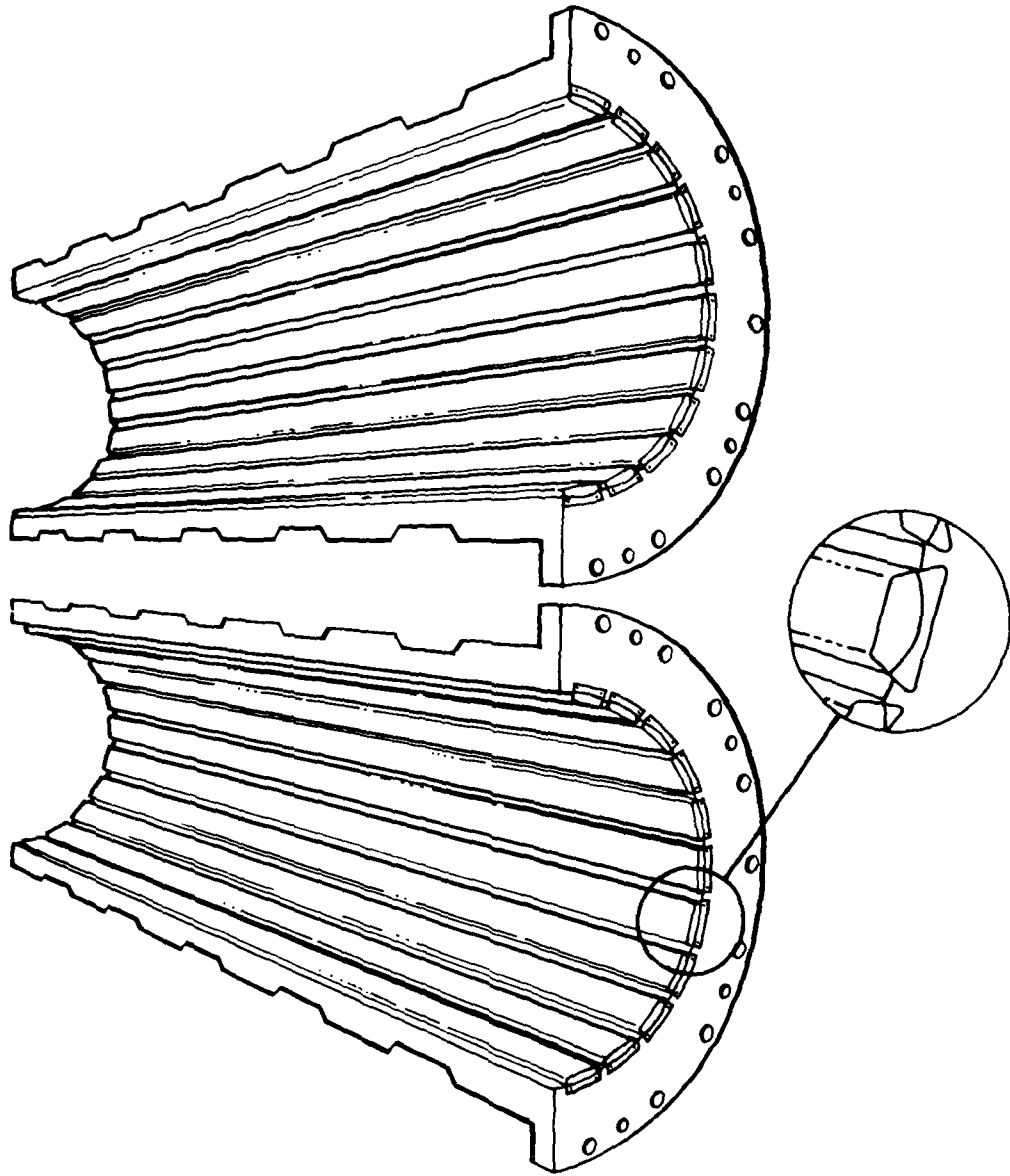


Figure 1 - Typical Bearing Construction

2. corrosion of the brass backing in the form of dezincification - resulting in loosening of staves in the dovetail slots, causing failure and degrading the bond at the rubber-brass interface; and

3. low-speed vibration caused by stick-slip motion under starved lubrication conditions.

Water-lubricated sterntube and strut bearings operate much of their lives in the boundary and mixed lubrication regions. That is, load is either carried completely or in part by actual contact between the surface of the bearing and the rotating mating shaft surface. Static or breakaway friction coefficients ordinarily fall in the range 0.4 to 0.7, although in some circumstances they may be higher. Deformation of compliant rubber surfaces is many times that of the lubricant film thickness. This compliance provides tolerance for passage of contaminants such as sand with minimal damage to the journal and bearing. Dynamic friction for conventional staves may be characterized by plotting the coefficient of friction against surface speed. Friction in a new bearing changes considerably when the bearing is first put into service.^{3,4} It is therefore essential to break in bearings before comparing results. Figure 2 shows typical dynamic friction results for water-lubricated stave bearings before and after break-in. Note that, at some critical speed, the friction increases suddenly. Operation in this region of friction change can result in stick-slip motion and resultant vibration. Use of the jacking gear often results in stick-slip motion.⁵ Important benefits can be gained by deferring the onset of the stick-slip phenomenon to a lower speed, under a given load. Such improvements are being explored herein through bearing stave design. It is the purpose of this report to compare the frictional characteristics of seven stave designs mounted in a full-complement bearing.

THEORETICAL BACKGROUND

To the authors' knowledge, there exists no hydrodynamic analysis of compliant surface stave bearings. However, some insight into their behavior can be obtained from developed expressions for rigid-surfaced hydrodynamic bearings. For a one-dimensional problem, Fuller⁶ developed the

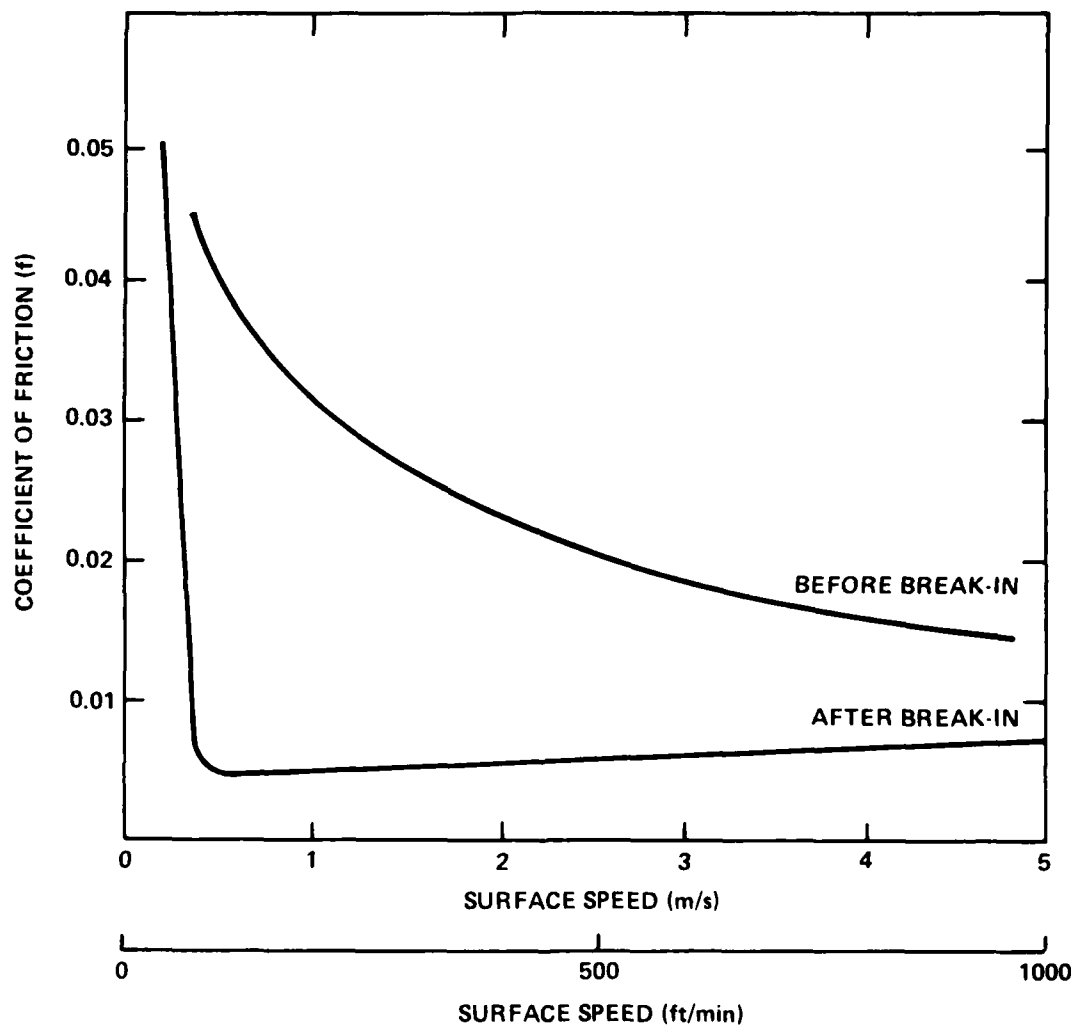


Figure 2 - Typical Dynamic Friction Coefficient for Water-Lubricated Stave Bearing Before and After Break-In

following expression relating the film thickness and the pressure obtained in the film

$$\frac{dp}{dx} = 6\mu U \left[\frac{h^* - h}{h^3} \right] \quad (1)$$

This equation is valid when the following conditions exist:

1. laminar flow conditions prevail and the liquids are Newtonian;
2. inertia forces are small as compared to viscous shear forces;
3. the fluid is incompressible;
4. the pressure in the film is a function only of x;
5. the velocity in the film is a function of both x and y; and
6. the viscosity of the liquid as it passes through the bearing

remains constant.

Equation (1) may be applied to rigid-surfaced bearings to determine the pressure buildup for any geometric shape or configuration if h can be described in terms of x.

For compliant-surfaced bearings such as the rubber-surfaced staves, a pressure is generated due to the elastic deformation in the rubber. The static pressure produced between a cylinder and a flat surface can be determined from the following formula⁷

$$p = \frac{2W}{\pi a} \left[1 - \left(\frac{x}{a} \right)^2 \right]^{1/2} \quad (2)$$

Hydrodynamic film generation is dependent upon the existence of a converging wedge of fluid in the direction of motion. Note that such a wedge of fluid is created due to increasing pressure over the first half of the contact of a cylinder (journal) on a flat surface (stave). The peak pressure and the rate of change of pressure with distance into the load region are dependent upon the width of the load zone. The width of the load zone is in turn dependent upon the applied load, the diameter of the journal,

the modulus of elasticity, and Poisson's ratio for each material according to Roark⁸ as

$$a = 0.8 \sqrt{WD \left(\frac{1-\nu_1^2}{E_1} + \frac{1-\nu_2^2}{E_2} \right)} \quad (3)$$

The stave designs being evaluated herein are intended to establish the relative importance of rubber hardness, rubber thickness, and the shape of the pressure profile in the load zone as they affect the friction characteristics of the bearing.

BEARING STAVE DESCRIPTION

All staves evaluated were 14.6 cm (5.75 in.) long. Figure 3 shows a cross-sectional view of each design. They will be referred to by Roman Numerals I through VII. Design I represents the standard configuration in use in most Navy ships today. The hardness of the rubber was 85'5 on the Shore A scale (instantaneous). The composition of the rubber is designated as *Composition A*. Design II was made of the same composition rubber, but the layer of rubber was only half the thickness of the standard stave design. Reducing rubber thickness increases the effective compressive modulus E, thereby reducing the width of contact (see Equation (3)). The peak pressure in the contact zone increases as indicated in Equation (2). Design III was identical to Design I except for the radius of the backing interface. Designs IV and V combine several factors. These designs were included because they presently are being evaluated in full-scale shipboard sterntube bearings. They are made commercially using a proprietary composition rubber (designated as *Composition B*). Both designs utilize thinner and softer rubber than that used in the conventional staves. Both are plastic backed and are of uniform rubber thickness. Stave designs VI and VII were included to evaluate the effect of nonsymmetrical pressure profile. They also use softer rubber than the composition used in the conventional staves. By Equation (2) it can be seen that the pressure profile for a conventional flat stave is parabolic

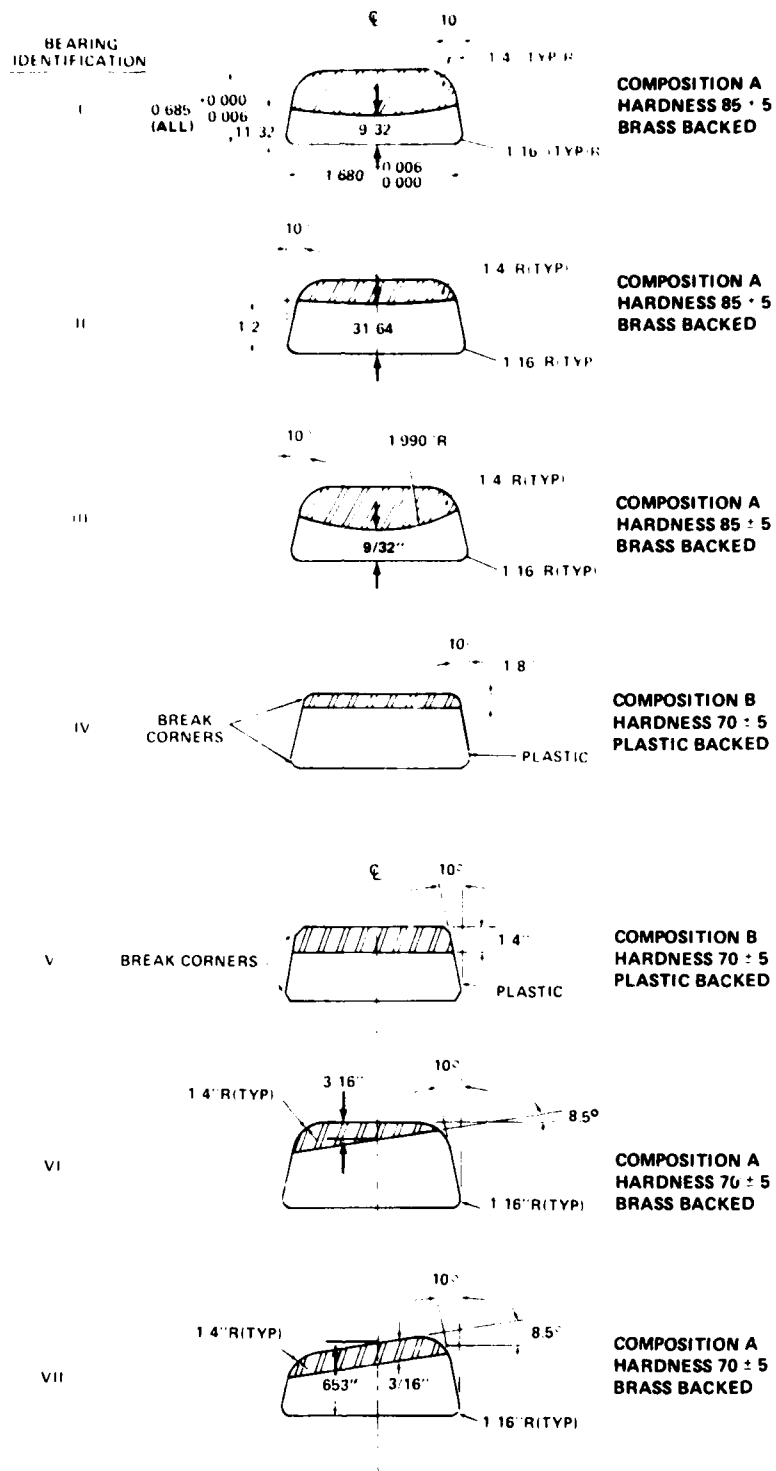


Figure 3 - Stave Configuration and Identification

and symmetrical about the center of contact which corresponds to the point of maximum pressure. In reality the pressure profile under dynamic conditions is skewed slightly toward the trailing edge. The contact with the shaft of Design VI occurs near the center of the stave width; however, the local stiffness in compression increases toward the trailing edge due to reduced rubber thickness. Hence, the pressure profile will be skewed additionally toward the trailing edge. The contact of Design VII occurs at or near the trailing edge. Inclination of the stave surface is expected to produce a different pressure profile than the conventional flat-surfaced stave.

TEST MACHINE

The test machine used to conduct these friction tests is shown in Figure 4. Its principal components consist of a drive motor, a right-angle gearbox, a torque sensor, a support housing, a hydraulic load cylinder, and a test chamber. The drive motor is a variable-speed unit with an upper limit of 400 rpm. It is coupled to a right-angle gearbox with a 1:1 ratio. The gearbox is connected to a 565 N-m (5000 lb-in.) torque sensor. Radial load is applied to the test bearing by the hydraulic load cylinder. The load is transmitted back to the frame through two grease-lubricated ball bearings contained in the support housing. A face seal in the support housing keeps water in the test chamber from entering the support housing. Figure 5 shows a top view of the test chamber with a test bearing in place. Load is transmitted from the load cylinder via an instrumented clevis pin through the load yoke and to the bearing. Load is applied to the lower half of the bearing. Rotation is in the counter-clockwise direction. The bearing housing was designed in accordance with Navy standard plans for a 17.15-cm (6 3/4-in.) O.D. shaft. Twelve staves of No. 1 size make up the full-complement bearing. The shaft is made of 70-30 copper-nickel. Fresh water is supplied to the test chamber. During the test the following parameters were monitored: shaft speed in revolutions per minute, radial load (load piston pressure and clevis pin load readout), torque, temperature of water, and date and time of test. Bearing load when expressed in kilopascals or pounds per square inch is based upon the projected area.

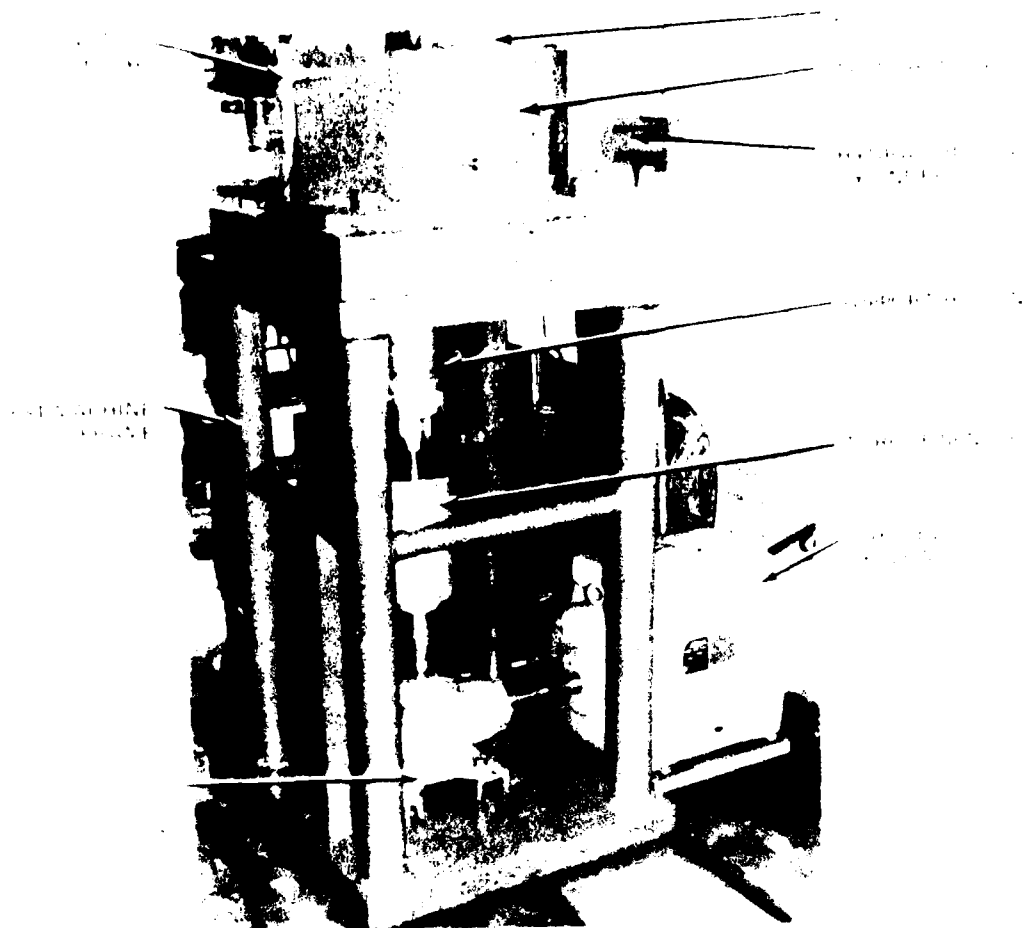


Figure 4 - Test Machine

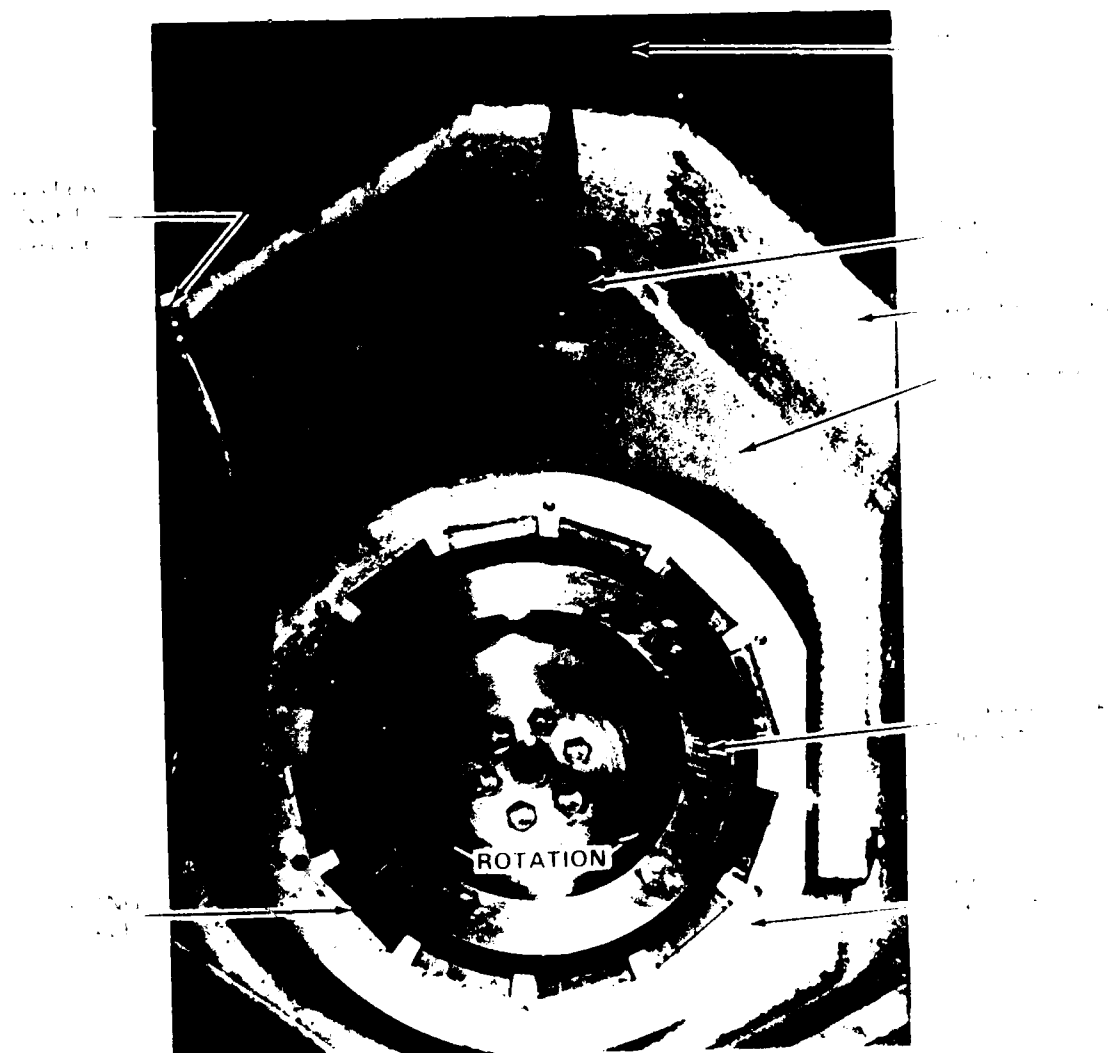


Figure 5 - Top View of Test Bearing

TEST PROCEDURE

All tests were conducted in the following sequence:

1. The staves were inserted into the dovetail housing, and the bore of the assembly was measured under controlled temperature and humidity conditions.
2. If the bearing clearance exceeded the 0.0012 to 0.0028 in. permitted by current Navy practice for this size shaft, the staves were shimmed accordingly and remeasured.
3. The shaft was polished to remove any sediments resulting from the water or rubber transfer remaining from a previous test. The polishing did not reduce the shaft diameter; it merely restored the surface finish of 12-20 μ in. (circumferentially) by removing foreign deposits.
4. Break-in tests were initiated. The machine was operated at 60 rpm and the load increased by 70 kPa (10 psi) in 15-min intervals until 280 kPa (40 psi) was reached.
5. This condition was held for 50 hr. Torque, speed, and water temperature were monitored and recorded.
6. The bearing was removed from the machine. Measurements of the width of the load track on each stave were made, and the load track pattern was photographed.
7. The bearing was reinstalled and operated at 60 rpm. The load was increased by 140-kPa (20-psi) increments every 15 min until 700 kPa (100 psi) was reached.
8. Steps 5 and 6 were repeated.
9. Dynamic tests were begun. The bearing was reinstalled, the machine was operated at 400 rpm, and a load of 70 kPa (10 psi) was applied for 15 min. Torque, speed, water temperature, and load were recorded. The speed was then reduced to 250, 100, 60, 40, 20, 10, and 5 rpm, respectively, for 15-min operation each, and the same data was recorded. The minimum speed achieved depended upon the torque limits of the drive motor.
10. Step 9 was repeated for 280 kPa (40 psi) and again for 700 kPa (100 psi).
11. Breakaway tests then were conducted. The shaft was manually rotated in both directions under no load to provide a film of lubricant between the bearing staves and the shaft.

12. A load of 280 kPa (40 psi) was applied. After the prescribed time elapsed, the shaft was manually rotated using a lever arm. The torque required to initiate rotation was recorded.

13. Step 12 was repeated for several time intervals. The time under load was randomly ordered.

RESULTS

The recorded torque, under dynamic conditions, was corrected by subtracting the tare torque contributed by the support bearings and the face seal. The method used to determine the magnitude of support bearing and face seal torque is presented in the Appendix. After correction for tare torque, the coefficient of friction was calculated using the formula

$$T = fPR \quad (4)$$

Values of the coefficient of friction were plotted versus operating speed for bearing loads of 70, 280, and 700 kPa (10, 40, and 100 psi, respectively). Breakaway friction coefficients were determined using the same formula, but no corrections for tare torque were made. Breakaway torque of the support bearings and seal is negligible compared with that of the test bearing. The breakaway coefficient of friction was plotted versus time under load. These tests were conducted under loads of 280 kPa (40 psi) only.

Figure 6 presents the results of dynamic tests on the conventional staves, set I. It represents typical performance of all stave designs considered herein. The seven bearing sets will be evaluated by comparing the minimum coefficient of friction values and by comparing the speed at which the dynamic coefficient of friction crosses a value of 0.01 for bearing loads of 280 and 700 kPa (40 and 100 psi), respectively. These parameters are presented in Table 1 for each bearing type. Sets VI and VII were also tested dynamically in the reverse direction, and results are given in Table 1.

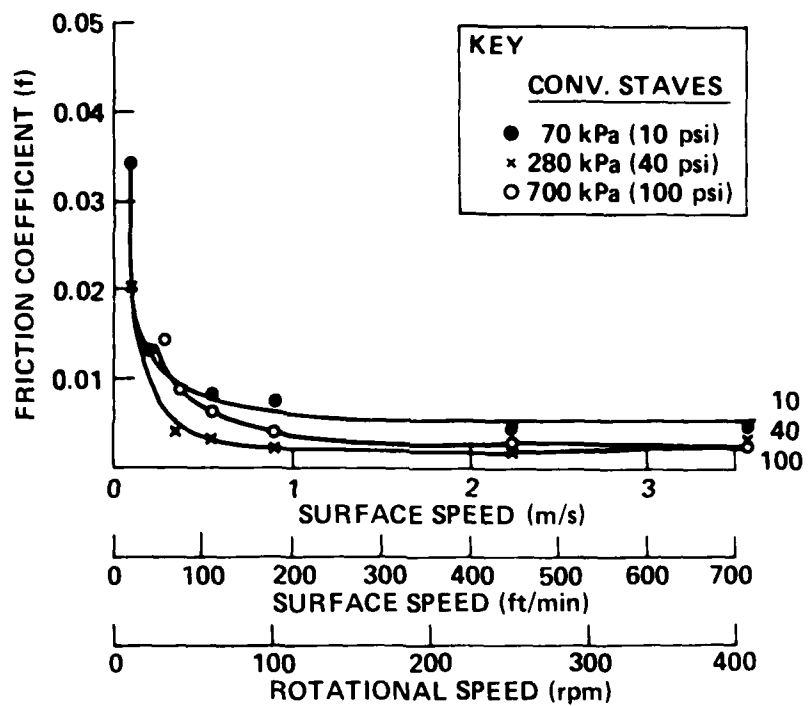


Figure 6 - Dynamic Friction Coefficient for Conventional Staves

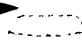
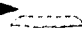
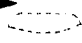
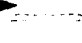
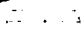
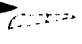
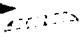
TABLE 1 - DYNAMIC FRICTION CHARACTERISTICS

Bearing Description	Stave Cross Section	Minimum Coefficient of Friction, f_{min}			Speed at Which $f = 0.01$				
		280 kPa (40 psi)	RR*	700 kPa (100 psi)	RR	280 kPa (40 psi)	RR	700 kPa (100 psi)	RR
I	ROT→	0.0021	5	0.0029	7	0.203 m/s (40 ft/min)	4	0.330 m/s (65 ft/min)	7
II	ROT→	0.0014	3	0.0016	2	0.228 (45)	6	0.304 (60)	4
III	ROT→	0.0012	2	0.0021	4	0.127 (25)	2	~0.127 (~25)	1
IV	ROT→	0.0019	4	0.0017	3	0.101 (20)	1	~0.127 (~25)	1
V	ROT→	0.0029	7	0.0028	6	0.203 (40)	4	0.304 (60)	4
VI	ROT→	0.0006	1	0.0015	1	0.177 (35)	3	~0.127 (~25)	1
VII	ROT→	0.0025	6	0.0021	4	0.304 (60)	7	0.304 (60)	4
VI	←ROT	0.0041	8	0.0036	8	0.355 (70)	8	(0.762) (150)	8
VII	←ROT	0.0332 (400 rpm)	9	Not Tested	9	>3.591 (>707)	9	Not Tested	9

*RR - Relative ranking.

Figure 7 presents the breakaway friction results of the conventional staves, Set I. It presents typical results for all stave designs. Figure 7 can be characterized by the value of the coefficient of friction under load for 5 min, the average friction coefficient under load between 4 and 6 hr, between 16 and 22 hr, and between 68 and 70 hr. Comparison of these magnitudes is presented in Table 2 for all seven stave designs.

TABLE 2 - STATIC COEFFICIENT OF FRICTION
UNDER 280-kPa (40-psi) LOAD

Bearing Description	Stave Cross Section	Time under Load							
		5 min	RR	4-6 hr	RR	16-22 hr	RR	68 hr	RR
I	ROT → 	0.44	2	0.65-0.68	4	0.71-0.75	6	0.87	6
II	ROT → 	0.47	3	0.63	3	0.60-0.66	3	0.60	2
III	ROT → 	0.60	5	0.75-0.77	7	0.74-0.81	7	0.90	7
IV	ROT → 	0.52	4	0.53	2	0.48-0.54	1	0.63	4
V	ROT → 	0.77	7	0.68	6	0.63-0.68	4	0.60	2
VI	ROT → 	0.61	6	0.66	4	0.66	4	0.69	5
VII	ROT → 	0.33	1	0.48	1	0.53	1	0.54	1

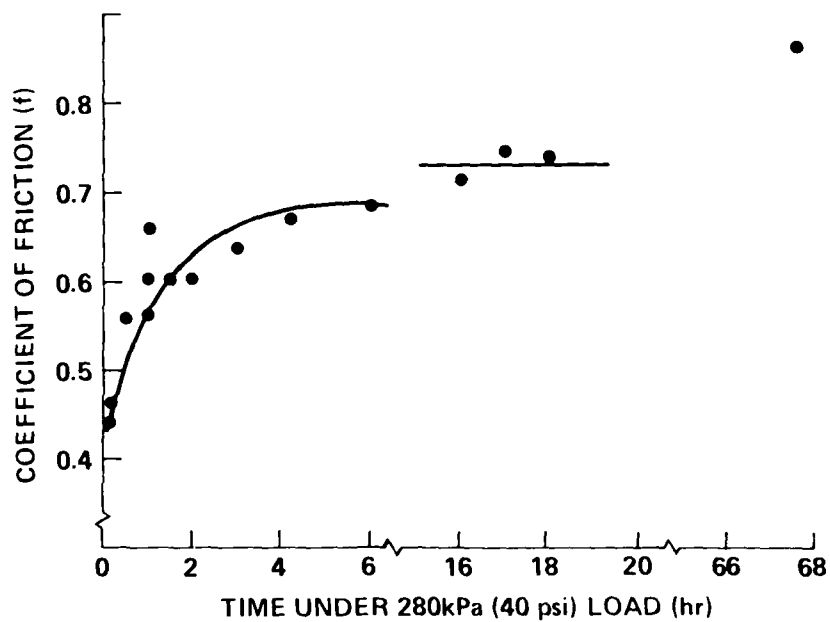


Figure 7 - Breakaway Friction versus Time under 280-kPa (40-psi) Load for Conventional Staves

Figure 8 shows a closeup of the conventional staves, Set I, after 50 hr at 60 rpm under 280 kPa (40 psi). The load distribution within the bearing assembly can be estimated using Equation (3), the measured width of the load pattern, and the properties of the materials. Figure 9 presents the distribution of load for Set I shown in Figure 8. This distribution is considered typical of all tests of the flat-surfaced staves.

DISCUSSION AND CONCLUSIONS

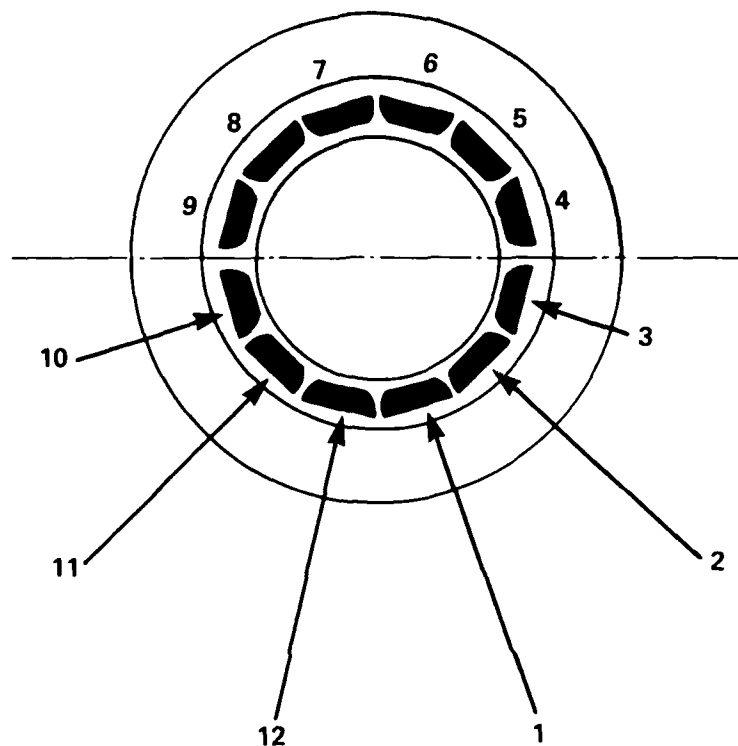
The data presented herein are intended to indicate the relative importance of parameters based upon trends. The magnitude of the minimum dynamic friction coefficients is not considered as good an indicator of dynamic performance as the speed at which a sudden increase in friction occurs. Therefore, the speed at which $f = 0.01$ was used to compare the dynamic performance of the stave designs. There appears to be no correlation between dynamic and breakaway friction. Design VII exhibited the lowest breakaway friction but had one of the highest dynamic friction.

Dynamic friction results using the speed at which $f = 0.01$ as a gauging factor indicate the following:

1. The thickness of a uniform layer of rubber has a significant effect on the friction. The only difference between Designs IV and V (being presently evaluated on shipboard) was the thickness of the rubber. The speed at which $f = 0.01$ for the thinner rubber stave was approximately half that of Design V.
2. Hardness of rubber does not seem to be an important parameter in dynamic friction. Designs II and V have rubber thicknesses of 0.51 and 0.64 cm (0.20 and 0.25 in.), respectively. Their primary differences are the rubber hardness, 85 ± 5 for Design II and 70 ± 5 for Design V. The speed at which $f = 0.01$ is about the same for both.
3. Geometrical configuration such as changing the radius to the backing-rubber interface may be important. The only difference between Designs I (conventional) and III is the radius to that interface. Design I radius is about 12.7 cm (5 in.) as compared with 5.1 cm (2 in.) for Design III. Performance is improved by a factor of 2 with the smaller radius.



Figure 8 - Load Pattern on Set 1 after 50-hr Break-In
at 60 rpm under 280-kPa (40-psi) Load



STAVE NO.	TRACK WIDTH (in)	NORMAL LOAD (lb)
1	0.78	553
2	0.60	327
3	0.18	30
10	0.38	131
11	0.60	327
12	0.76	553

Figure 9 - Track Width and Load Distribution for Set 1 after 50-hr Break-In at 60 rpm and 280-kPa (40-psi) Load

Design V did not yield much of an improvement as compared to the conventional bearing I despite the reduction in rubber thickness from 1.02 to 0.64 cm (0.40 to 0.25 in.). This may be attributed to the differences in radius to the rubber-backing interface.

Designs VI and VII also indicate that the geometry plays an important role in the dynamic behavior of bearing staves. It is suspected that the shape of the pressure profile generated between the bearing and most heavily loaded stave is the controlling factor. This is also affected by the thickness, hardness, and properties of the rubber. When Designs VI and VII were operated in the reverse direction (producing a negative pressure gradient), very poor results were obtained.

The tests presented in this report were conducted under standardized and controlled conditions. Each bearing set was given break-in tests after which it was assumed that the performance was representative of its design. No levels of significance therefore were established. The intent of this report was to indicate potential merits of different designs. Time restraints did not permit repeatability runs. However, it is recommended that more detailed testing be conducted and that repeatability tests be included.

APPENDIX

CORRECTION TORQUE CALCULATION

The torque sensed by the torquemeter in the test machine consists of that required to rotate the shaft in the test bearing, the two support ball bearings, and the face seal. To obtain the test bearing torque, the torque from the support bearings and face seal must be deducted from the recorded magnitude. These corrections were determined in the following manner. The test bearing was replaced with a size 314 deep-groove ball bearing (calibration bearing). It was lubricated with the same grease used in the support bearings. The test shaft was rotated to channel the grease until the torque required reached a steady value. Torque was recorded under the loads and speeds to be used in the stave bearing tests. The bearing and seal arrangement are shown schematically in Figure 10. The tare torque consists of the torque from the two support bearings and the face seal. The friction losses in ball bearings can generally be expressed⁹ as follows

$$T = T_L + T_V \quad (5)$$

T_L is the load torque and is a function of load, bearing size, bearing type, and the direction of load. T_V is the viscous torque and is a function of the lubricant and bearing size.

The magnitude of the radial loads on the support bearings can be determined from Figure 10 by taking moments about the 214 bearing

$$15P - 6R_1 = 0$$

$$R_1 = 2.5P \quad (6)$$

$$R_2 = 1.5P$$

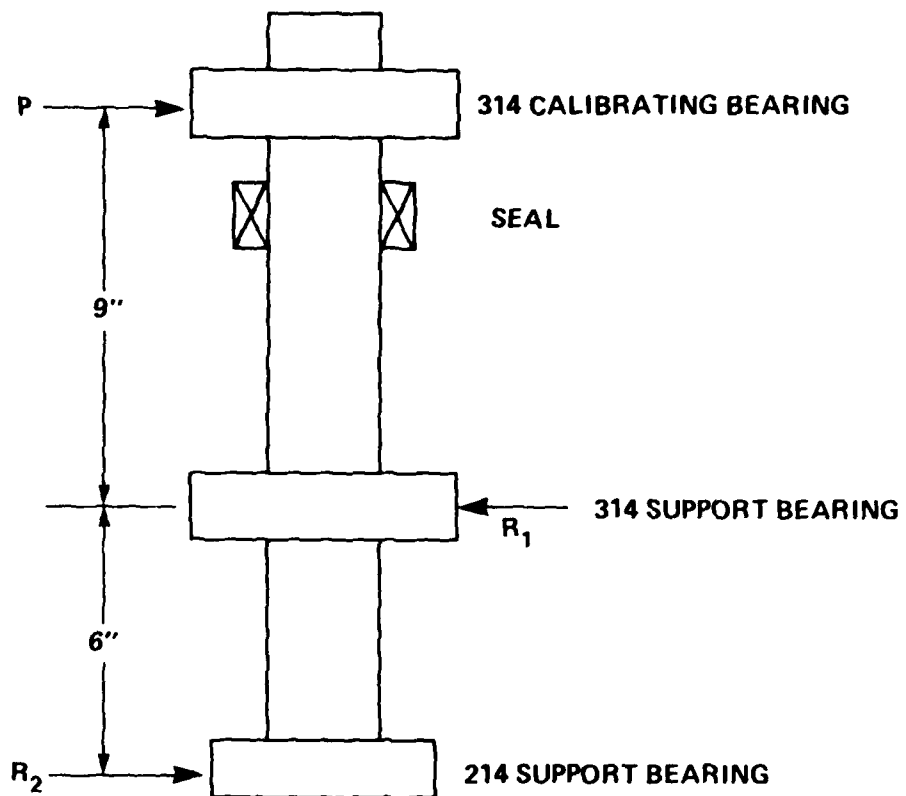


Figure 10 - Support Bearing and Seal Arrangement

The viscous contribution to the bearing torque was negligible compared with the load portion. Since the bearings were all deep-groove ball bearings and were loaded radially, the torque T_L is a function of applied load. The load on the calibration bearing is therefore 1/5 the total bearing load. $T_{CB} = 1.5T_B$

$$T_{TARE} = T_{SB} + T_S = T_T - 1/5 T_B$$

and

$$T_B = T_T - T_S$$

$$T_{TARE} = T_T - 1/5 (T_T - T_S)$$

$$T_{TARE} = 4/5 T_T + \frac{T_S}{5} \quad (7)$$

The seal friction was calculated in accordance with Mayer¹⁰ using a coefficient of friction of 0.25 and entered into Equation (7) to yield (expressed in lb-in.)

$$T_{TARE} = 4/5 T_T + 0.05 \quad (8)$$

Results of the runs with the calibration bearing were inserted into this equation. The resulting values of tare torque were plotted versus load and speed conditions and were used to determine the actual test bearing torque from the total measured torque.

REFERENCES

1. Smith, W.V. and L.G. Schneider, "Lubrication in a Sea-Water Environment," Naval Engineers Journal, pp. 841-854 (Oct 1963).
2. "Bearing Components, Bonded Synthetic Rubber, Water Lubricated," Military Specification MIL-B-17901 (3 Apr 1963).
3. Beatty, J.R. and D.H. Cornell, "Laboratory Testing Rubber Bearings - I," Rubber World (Dec 1949).
4. Beatty, J.R. and D.H. Cornell, "Laboratory Testing Rubber Bearings - II," Rubber World (Dec 1949).
5. Padden, R.R., "Slow Speed Propulsion Shaft Noises," NAVSHIPS Tech News (Dec 1973).
6. Fuller, D.D., "Theory and Practice of Lubrication for Engineers," John Wiley & Sons, New York (1956), pp. 150-154.
7. Moore, D., "The Friction and Lubrication of Elastomers," Pergamon Press Ltd. (1972), p. 53.
8. Roark, R., "Formulas for Stress and Strain," McGraw-Hill Book Co., Inc. (1938), p. 244.
9. Harris, T., "Rolling Bearing Analysis," John Wiley & Sons, Inc., New York (1966), pp. 446-451.
10. Mayer, E., "Leakage and Wear in Mechanical Seals," Machine Design (3 Mar 1960).

INITIAL DISTRIBUTION

Copies

6 NAVSEA
 1 SEA 05D
 1 SEA 05H
 1 SEA 05R
 1 SEA 524
 2 SEA 99612

12 DTIC

CENTER DISTRIBUTION

Copies	Code	Name
1	01	A. Powell
1	012.3	R. Allen
1	2802	I. Kramer
1	283	G. Bosmajian
16	2832	J. Dray
10	5211.1	Repts Dist
1	522.1	Unclass Lib (C)
1	522.2	Unclass Lib (A)
2	5231	Office Services